PCCP

PAPER

Cite this: *Phys. Chem. Chem. Phys.*, 2015, **17**, 27806

Investigation of field effects in a solid-state nanopore transistor†

Yong Youn and Seungwu Han*

Received 30th May 2015,
Accepted 23rd September 2015

DOI: 10.1039/c5cp03125g

www.rsc.org/pccp

In order to calculate ion currents through solid-state nanopore transistors realistically, we propose a computational model based on the Poisson–Nernst–Plank equation. In the present model, we determine the surface charge density locally on the nanopore by imposing consistency between the ion distribution and the chemical reaction at the surface. The model can consider a non-uniform influence by the gate voltage on the inner surface of the nanopore membrane, which enables us to investigate ion currents depending on the gate geometry such as the thickness and vertical position within the nanopore. We verify the validity of the model by comparing the pH dependence of simulation results with the extant experimental results. We also investigate the transistor behaviour depending on the surface material, pore geometry and gate position. In particular, we propose an optimized system to enhance the on/off ratio of the nanopore transistor.

Introduction

Nanopores have been used in various applications, notably in DNA sequencing[1–6] and bio-sensing.[7–10] Since the dimensions of nanopores are comparable to the Debye length in solution, the ion distribution and ion transport through nanopores depend on the surface charge density on the nanopore wall. For example, it is known that the pH conditions or ion concentration affect the charge density on the nanopore wall,[11–15] which in turn slows down the translocation speed of DNA.[5,16–18]

Recently, it has been proposed that the surface charge density can be electrically controlled by embedding the gate electrode inside the solid-state nanopore, reminiscent of the metal–oxide–semiconductor field-effect transistor (MOSFET) in microelectronic devices.[19–27] In a solid-state nanopore transistor, the gate potential affects the electric-double layer (EDL) by modifying the charge groups on the surface as well as the nearby ion concentration. The nanopore transistor has an advantage that it can control the ionic transport precisely and instantaneously. Furthermore, in combination with an ionic diode,[28–30] it can manipulate, switch, redirect, and amplify the signal, realizing full-blown ionic circuits that mimic the electronic counterparts.[21] Several experiments have demonstrated the usefulness of nanopore transistors.[25,26] For example, in ref. 25, the translocation speed of DNA was reduced by 20-fold in the "off" state of the transistor. Furthermore, the capture rate of DNA was also enhanced.[26] However, more dramatic improvements are in demand for detecting individual base pairs.

Computational modeling is the favored method for understanding the working principle of nanopore transistors as well as for designing a promising device structure. So far, various theoretical models[31–37] have been suggested to understand the gate effect in nanopores. However, each model has certain limitations that originate from the underlying approximations. For instance, the modulation of the surface charge density was neglected in ref. 31–34. More recent models consider the variation of the surface charge density with respect to the gate voltage.[35–37] However, they still treat the gate effect within the one-dimensional model and so neglect the non-uniformity of the surface potential on the inner wall, which becomes significant when the gate electrode is thinner than the nanopore membrane. Furthermore, the models calculate the potential distribution within the EDL by using the Grahame equation that precludes overlapping EDLs. This compromises the computational accuracy when the thickness of the EDL is larger than the pore radius.

In this study, we develop a numerical model of a nanopore transistor that explicitly considers the finite thickness of the gate electrode within the nanopore membrane. The present model calculates the potential distribution in the membrane based on the Poisson–Nernst–Planck (PNP) model.[38–40] The surface charge density is determined by imposing self-consistency among the ion distribution near the surface and the chemical reaction of the surface hydroxyl groups.[41,42] Using the proposed computational model, we investigate the transistor behavior depending on the surface material, pore geometry and gate position. Based on the results, we propose a way to enhance the on/off ratio of a nanopore transistor by modifying the gate geometry.

Department of materials Science and Engineering and Research Institute of Advanced Materials, Seoul National University, Seoul 151-744, Korea. E-mail: hansw@snu.ac.kr

† Electronic supplementary information (ESI) available. See DOI: 10.1039/c5cp03125g

Model

As a model system, we assume a cylindrical nanopore transistor in which the gate electrode is embedded and the surface is covered by oxide. Fig. 1 shows the material structure and the simulation domains of a typical gate-embedded conical nanopore transistor. The boundary conditions in the PNP equation are compiled in Table 1 for each boundary numbered in the figure. Since the dimension of the reservoir is sufficiently large, ions do not flow along the radial direction on boundary 2 and 8, resulting in the no-flux and zero-charge boundary conditions.[38–40] In the present model, electric potentials within not only the electrolyte but also the membrane (dielectric films and oxides) are explicitly computed. On the other hand, the Nernst–Plank equation is the governing equation in solution that produces the ion distribution and flow. We impose the axial symmetry and solve the PNP equation in the 2-dimensional space.

The reactive groups on the oxide surface are in chemical equilibrium with the solution, which dictates their charge states. Here we assume that the hydroxyl group is the sole reactive group on the surface and it undergoes the following chemical reactions:[41–45]

$$\mathrm{R{\cdot}OH} \leftrightarrow \mathrm{R{\cdot}O^-} + \mathrm{H^+} \quad (1)$$

$$\mathrm{R{\cdot}OH_2^+} \leftrightarrow \mathrm{R{\cdot}OH} + \mathrm{H^+}, \quad (2)$$

where R indicates the metal atom in the oxide surface. The surface charge density (σ_{chem}) at the specific position of $\mathbf{r}_s$ on the surface is given by

$$\sigma_{\mathrm{chem}}(\mathbf{r}_s) = e\Gamma^{\mathrm{OH_2^+}}(\mathbf{r}_s) - e\Gamma^{\mathrm{O^-}}(\mathbf{r}_s) \quad (3)$$

where $\Gamma^{\mathrm{OH_2^+}}(\mathbf{r}_s)$ and $\Gamma^{\mathrm{O^-}}(\mathbf{r}_s)$ are the densities of $\mathrm{OH_2^+}$ and $\mathrm{O^-}$ groups at $\mathbf{r}_s$ on the surface, respectively, and e is the electron charge (positive). Since the density of reactive groups (Γ) is roughly constant over the surface, the following relation holds:

$$\Gamma = \Gamma^{\mathrm{OH_2^+}}(\mathbf{r}_s) + \Gamma^{\mathrm{OH}}(\mathbf{r}_s) + \Gamma^{\mathrm{O^-}}(\mathbf{r}_s). \quad (4)$$

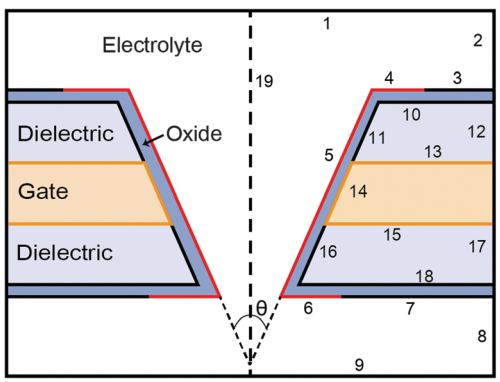

Fig. 1 Schematic of the nanopore used for the PNP model. The sketch illustrates the electrolyte, oxide material, dielectric films, charged surface of the membrane (red, surface 4–6), gate/membrane interface (orange, surface 13–15) and axial symmetry line (dashed line, surface 19). The pore angle (θ) is also defined.

Table 1 Boundary conditions for governing equations

Surface	Nernst–Planck equation	Poisson equation
1	Concentration, $c_i = c_0$	Electric potential, $V = V_D$ (=−1 V)
2, 3, 7, 8	No flux, $-\mathbf{n}\cdot\mathbf{N}_i = 0$	Zero charge, $\mathbf{n}\cdot\mathbf{D} = 0$
4–6	No flux, $-\mathbf{n}\cdot\mathbf{N}_i = 0$	Surface charge, $\mathbf{n}\cdot(\mathbf{D}_1 - \mathbf{D}_2) = \sigma$
9	Concentration, $c_i = c_0$	Ground, $V = 0$
19	Axial symmetry	Axial symmetry
13–16		Electric potential, $V = V_G$
10–12, 16–18		Zero charge, $\mathbf{n}\cdot\mathbf{D} = 0$

c_i: ion concentration of the ith ionic species; c_0: bulk concentration; $\mathbf{n}$: vector normal to the surface; $\mathbf{N}_i$: ionic flux of the ith ionic species; V_D: drain potential; $\mathbf{D}$: electric displacement field; σ: surface charge density; V_G: gate potential.

With pK_1 and pK_2 as equilibrium constants corresponding to the chemical reaction in eqn (1) and (2), respectively, the ratios of the charged reactive groups satisfy the following mass-action laws:

$$10^{-pK_1} = \frac{[\mathrm{H^+}]_s\Gamma^{\mathrm{O^-}}}{\Gamma^{\mathrm{OH}}} \quad (5)$$

$$10^{-pK_2} = \frac{[\mathrm{H^+}]_s\Gamma^{\mathrm{OH}}}{\Gamma^{\mathrm{OH_2^+}}}, \quad (6)$$

where $[\mathrm{H^+}]_s$ indicates hydrogen activity close to $\mathbf{r}_s$. From eqn (3)–(6), σ_{chem} relates to $[\mathrm{H^+}]_s$ as follows:

$$\sigma_{\mathrm{chem}} = e\Gamma\left[\left(1 + \frac{10^{-pK_2}}{[\mathrm{H^+}]_s} + \frac{10^{-pK_1}10^{-pK_2}}{[\mathrm{H^+}]_s[\mathrm{H^+}]_s}\right)^{-1} - \left(1 + \frac{[\mathrm{H^+}]_s}{10^{-pK_1}} + \frac{[\mathrm{H^+}]_s[\mathrm{H^+}]_s}{10^{-pK_1}10^{-pK_2}}\right)^{-1}\right] \quad (7)$$

On the other hand, the ratio between $[\mathrm{H^+}]_s$ and $[\mathrm{H^+}]_0$, the hydrogen activity in the bulk solution, is the same as that between $(c_+)_s$ and $(c_+)_0$, the corresponding cation concentrations, because they lie at the same electrostatic potential. That is to say,

$$[\mathrm{H^+}]_s = \frac{[\mathrm{H^+}]_0(c_+)_s}{(c_+)_0} = \frac{10^{-\mathrm{pH}}(c_+)_s}{(c_+)_0}. \quad (8)$$

It is evident that eqn (7) and (8) are related self-consistently; for the given $\sigma^{\mathrm{in}}_{\mathrm{chem}}(\mathbf{r}_s)$, the PNP model brings forth $(c_+)_s$. Then, $[\mathrm{H^+}]_s$ is obtained through eqn (8), which in turn gives $\sigma^{\mathrm{out}}_{\mathrm{chem}}(\mathbf{r}_s)$ from eqn (7). $\sigma^{\mathrm{out}}_{\mathrm{chem}}(\mathbf{r}_s)$ should match with $\sigma^{\mathrm{in}}_{\mathrm{chem}}(\mathbf{r}_s)$, leading to the self-consistency conditions. We recall that σ_{chem}, $[\mathrm{H^+}]_s$ and $(c_+)_s$ are all local functions that depend on $\mathbf{r}_s$. The self-consistency cycle determines $\sigma_{\mathrm{chem}}(\mathbf{r}_s)$ together with the ion current flowing through the nanopore transistor.

Results and discussions

In this section, we present the computational results on the ion current of the nanopore transistor based on the theoretical model proposed in the previous section. We employ the COMSOL Multiphysics program throughout this study. The ion concentration is set to 0.1 mM KCl and we fix some geometrical parameters for the convenience of comparison; a narrow diameter

of the pore (20 nm), pore length (500 nm), thickness of the gate electrode (100 nm), and thickness of oxide layer (5 nm). The diffusion coefficient of K^+ and Cl^- are 1.95×10^{-9} m^2 s^{-1} and 2.03×10^{-9} m^2 s^{-1}, respectively. The applied source–drain voltage is −1 V, *i.e.*, K^+ flows from the bottom to top reservoirs. We applied a wide range of gate voltages, from −3 to 3 V, to show the influence of the gate potential clearly. The maximum electric field in our simulation is comparable to the typical dielectric strength of the oxides. Therefore, the comparison with experiments should be made on the smaller voltage range. The channel dielectric materials are SiO_2 or Al_2O_3, which are widely used in experiments. The pK_1/pK_2 values of SiO_2 and Al_2O_3 are 7.5/−2[42–44] and 9.5/4.4,[41] respectively. The density of the chemical reaction groups of SiO_2 and Al_2O_3 is assumed to be 8×10^{-18} m^{-2}.[35]

pH dependence

In order to check the validity of the present model, we first reproduce the pH dependence of the ion current in the nanopore transistor, which was already examined in ref. 20, 25 and 45. In experiments, either monotonic[20] or unipolar[45] behaviour was found when the gate potential changes its sign. (The dielectric material was SiO_2 in both experiments.) The difference originates from the pH conditions of the solution. Fig. 2 shows the computed ion current *versus* gate voltage of the straight nanopore transistor under different pH conditions of 5 and 7. We recall that the SiO_2 surface is negatively charged in both pH 5 and 7 solutions. Since it is negatively charged, the concentration of positive ions inside the pore is much higher than that of negative ions, and so the number of positive ions is a critical parameter governing the ion current. This also results in the p-type behaviour.

The inset figures in Fig. 2 show the positive ion concentration inside the pore. The ion current is modulated according to the gate voltage. When the negative gate potential is applied, the number of K^+ around the gate increases, resulting in a larger ion current under both pH conditions. In contrast, the positive gate reduces the K^+ concentration around the gate region and hence the ionic current.

In Fig. 2, the off state is observed only under the pH 5 conditions where the oxide surface is negatively charged in small amounts under the zero gate potential. In this case, the concentration of K^+ ions screening the surface charge is also small. The positive gate potential then easily repels K^+ ions from the nanopore, reducing the ion currents close to zero. On the other hand, if the oxide surface is more negatively charged as in the pH 7 solution, K^+ ions still remain around the gate in spite of the positive gate, and the off state is not achieved. These results are consistent with the experiment; in the acidic solution, a unipolar behaviour is observed and the ion current shows a monotonic behaviour under pH 7 conditions.

To examine the influence of ion concentrations, we compare the results under two different ion concentrations, 0.1 and 1 mM in Fig. S1 in the ESI.† It is clear that the transistor-like behavior is maintained even at the higher KCl concentration. However, the on/off ratio under the 0.1 mM conditions is larger than that under the 1 mM conditions. This is because at the low ion concentration, the EDL related to the ion concentration inside the pore becomes thicker so the influence of the gate potential becomes larger.

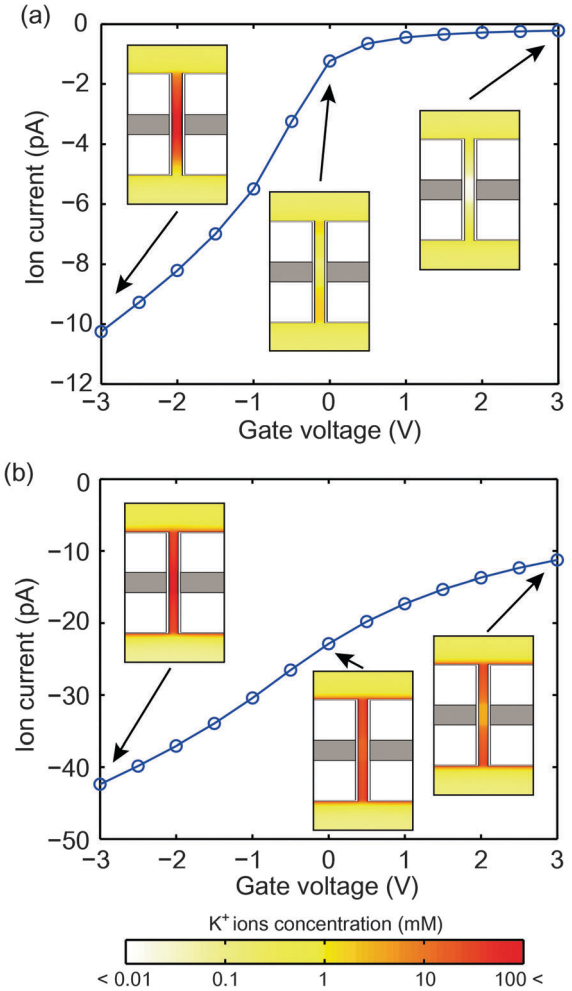

Fig. 2 Ion current *versus* gate voltage under (a) pH 5, (b) pH 7 conditions. Inset figures show the K^+ ion distribution. The gate electrode inside the nanopore membrane is shown as shaded regions.

In passing, we compare the present model with the prefixed surface charge model on the typical transistor-like behaviour in Fig. 2a. The results are shown in Fig. S2 in the ESI.† In the prefixed model, a bipolar behavior was found, which is not consistent with the experimental results. This indicates that the variation of the surface charge is critical for realistic simulations.

Effect of oxide materials

Next, we compare the p-type transistor behaviour and related properties depending on the oxide material covering the nanopore. This part was motivated by recent experiments showing that the ion current responds differently to the gate voltage depending on the material of the gate oxides.[34,45,46] In the previous studies,[47] σ_{chem} under zero gate potential was used in explaining the material dependence. However, the gate-induced modulation in σ_{chem} should also be included because it also

affects the response of the ion current significantly. In order to show the effect of the gate oxide, we consider SiO_2 and Al_2O_3, which are widely used in experiments. To compare fairly the influence of the gate potential, we adjust the pH value such that the surface charge densities on both oxides are the same under the zero gate potential. This is achieved with pH values of 5 and 7.6 for SiO_2 and Al_2O_3, respectively.

Fig. 3a shows the ion currents as a function of the gate voltage when SiO_2 and Al_2O_3 cover the nanopore. It is seen that the ion current in Al_2O_3 is less sensitive to the modulation of the gate voltage than that in SiO_2. These behaviours can be explained from the response of the surface potential and σ_{chem} to the gate voltage as shown in Fig. 3b and c. In Fig. 3b, the surface potential of Al_2O_3 changes within a narrow range in comparison with that of SiO_2, which results in the limited response as shown in Fig. 3a.

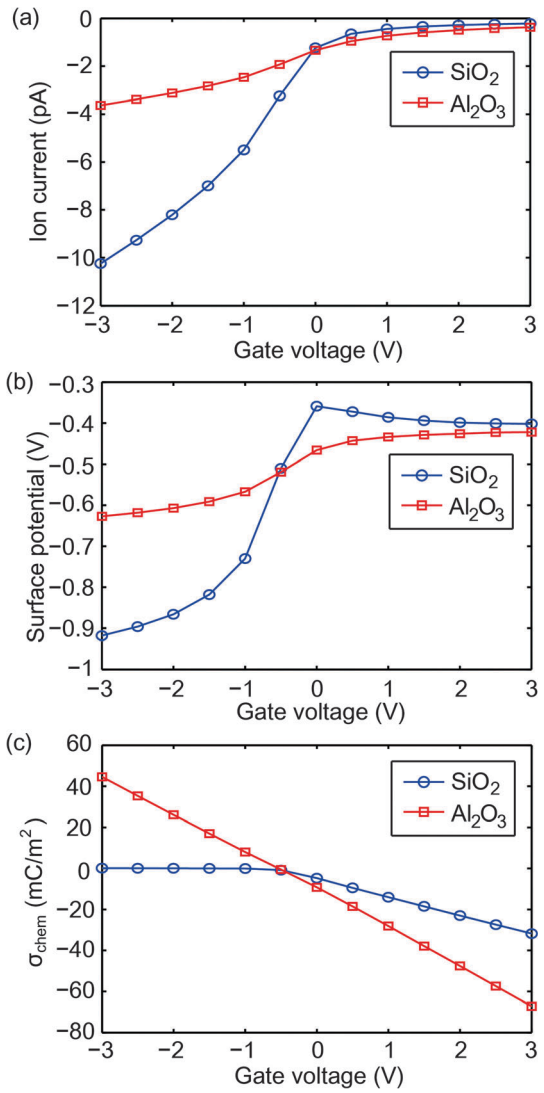

Fig. 3 (a) Ion current, (b) surface potential, and (c) surface charge density (σ_{chem}) with respect to the gate voltage for SiO_2 and Al_2O_3. Surface charge density and potential at the surface are calculated at the middle position of the gate electrode.

Several factors such as the gate voltage, the dielectric constant of the oxide, and chemical groups affect the surface potential. From the detailed analysis, we find that the modulation of σ_{chem} is the dominant factor in the present case. In Fig. 3c, it is seen that σ_{chem} in Al_2O_3 changes linearly and more widely than that of SiO_2. According to eqn (7), the pK and pH values determine the sign and magnitude of the surface charge. The pK_1 (9.5) and pK_2 (4.4) values of Al_2O_3 are relatively close to the pH value (7.5), indicating that the surface reactive groups readily assume positive or negative charges in response to the gate potential. The facile variation of σ_{chem} on Al_2O_3 can effectively screen the gate potential, weakening its influence on the ion distribution. In contrast, the SiO_2 surface can be only negatively charged under the given pH conditions due to the large difference between the pK_2 (−2) and pH conditions (5), resulting in the non-linear behaviour of σ_{chem}. The present results demonstrate that the current–voltage characteristics of nanopore transistors can be controlled by selecting gate oxides with appropriate pK values.

Influence of device geometry

In this subsection, we study the transistor-like behaviour based on the device geometry. Specifically, we try to maximize the on/off ratio, a critical device parameter for a transistor, by changing the position of the gate electrode and the pore angle. We limit the simulation conditions to the pH 5 solution and SiO_2 as the oxide layer. First, we show in Fig. 4a the current *versus* gate voltage depending on the position of the gate electrode. When the position of the gate electrode moves from the middle of the membrane (h = 250 nm) to near the outer membrane at the bottom (h = 60 nm), the on current increases while the off current decreases, enhancing the on/off ratio monotonically, as can be seen in Fig. 4b.

To explain the dependence on the gate position as mentioned above, we analyze the ion concentration inside the pore. Fig. 4c shows the colour maps for the K^+ and Cl^- concentrations on a plane perpendicular to the membrane for gate voltages of ±3 V and at center/bottom gate positions. When the gate electrode is placed in the middle of the membrane, the gate potential only affects the ion distribution inside the pore. If the gate position is lowered from 250 to 60 nm, the gate potential affects the salt concentration on broader regions including the pore entrances, in particular at the bottom. This is because the gate electrode influences the potential of the electrolyte near the bottom side of the membrane. Since the negative drain potential pulls K^+ ions from the bottom to the top reservoir, the on current increases. The on/off ratio is further enhanced by reducing the K^+ ions near the pore entrance under the positive gate potential. Therefore, the gate electrode placed near the lower side of the membrane produces larger on/off ratios. On the other hand, when the gate electrode is placed near the top side of the membrane, we find that the on/off ratio is reduced compared with that of the middle position, which can be easily understood from the foregoing discussions.

Next, to further enhance on/off ratio, we modify the pore angle of the nanopore (θ) while the gate electrode is fixed at the bottom region (see Fig. 1). The gate dependent ion currents are

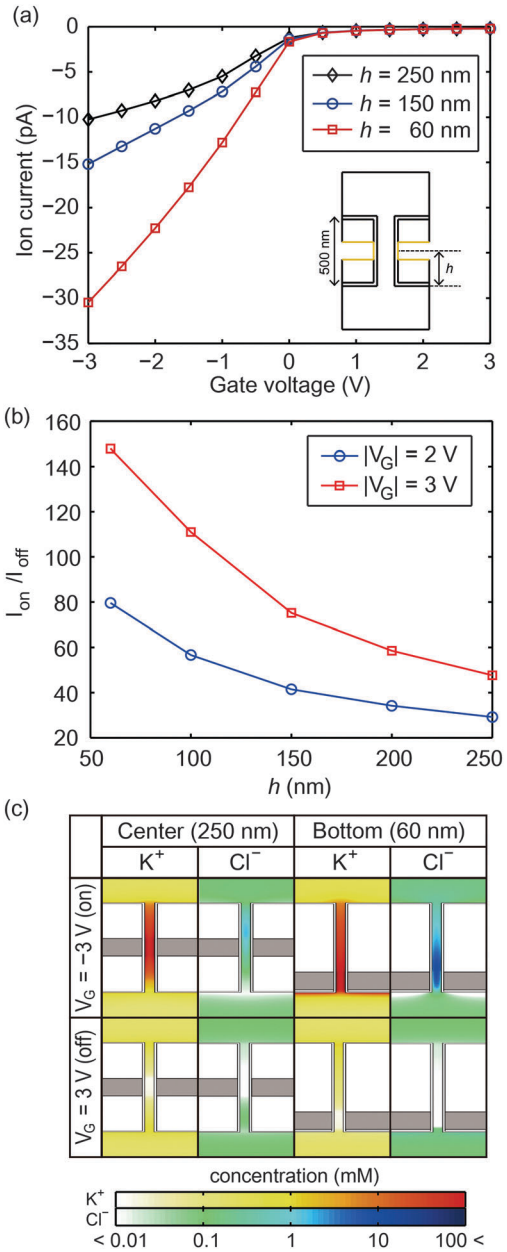

Fig. 4 (a) Ion current *versus* gate voltage depending on the position of the gate electrode. The inset shows the position of the gate electrode. (b) The on/off ratio with respect to the gate position when the magnitude of gate potential is 2 or 3 V. (c) Ion distribution depending on the gate potential and the position of gate electrode. The gate electrode inside the nanopore membrane is shown as shaded regions.

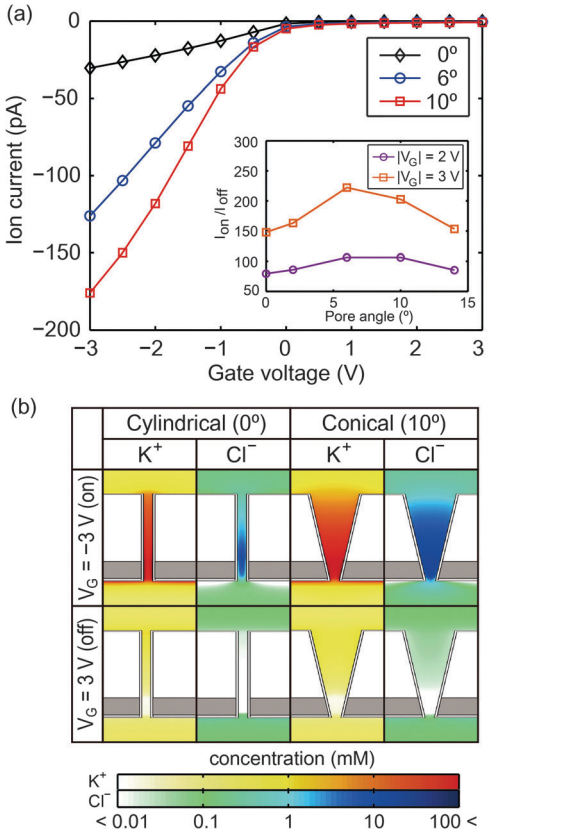

Fig. 5 (a) Ion current *vs.* gate voltage depending on the pore angle. Inset in (a) is the on/off ratio with respect to the pore angle when the magnitude of gate potential is 2 or 3 V. (b) Ion distribution depending on the gate potential and pore angle. The gate electrode inside the nanopore membrane is shown as shaded regions.

shown in Fig. 5a. In contrast to the gate position in the above, increasing the pore angle does not lead to the monotonous change in the on/off ratio as shown in the inset, and the on/off ratio peaks at a specific angle.

When the pore angle opens up, both on and off currents increase and so the on/off ratio varies depending on the relative increase rate. In the low-angle region ($\theta < 6^\circ$), the increase of the on current is larger than that of the off current, which can be understood by the ion distribution shown in Fig. 5b in the case of straight pore ($\theta = 0^\circ$). When the pore angle is small, it is difficult for ions to pass through the narrow pore under the positive gate potential, which hinders the enhancement of the off current. Thus, the on/off ratio increases as the pore angle becomes bigger. As the pore angle exceeds the optimal value, however, the increase in the number of ions moving through the pore in the off state is larger than that in the on state, leading to the decrease in the on/off ratio. Consequently, the on/off ratio peaked at around 6°.

Conclusion

In summary, we proposed a computational model to simulate the effect of the gate potential in a gate-embedded nanopore. The main improvement over previous work is that the present model calculates the surface charge density locally, extending its applicability to a wide range of nanopore transistors. By solving the model numerically, we showed that unipolar behaviour is observed at the SiO_2 surface under pH 5 conditions. In addition, by comparing the response of the ion current in different gate oxides, we demonstrated that the current–voltage characteristics of nanopore transistors can be controlled by selecting gate oxides with appropriate pK values. We also optimized the geometry such as the gate position and pore angle to maximize

the on/off current ratios. Our results showed that the geometric effect and the chemical reaction can be tuned to control the transistor-like behaviour of the ion current. We believe that the present model can be widely used in research of nanopore transistors.

Acknowledgements

We thank Prof. Wonmuk Hwang for helpful discussions. This work was supported by the Pioneer Research Center Program through the National Research Foundation of Korea funded by the Ministry of Education, Science and Technology (2012-0009563). The computations were carried out at KISTI (No. KSC-2014-C3-012).

Notes and references

1 V. Dimitrov, U. Mirsaidov, D. Wang, T. Sorsch, W. Mansfield, J. Miner, F. Klemens, R. Cirelli, S. Yemenicioglu and G. Timp, *Nanotechnology*, 2010, **21**, 065502.
2 B. M. Venkatesan, B. Dorvel, S. Yemenicioglu, N. Watkins, I. Petro and R. Bashir, *Adv. Mater.*, 2009, **21**, 2771–2776.
3 J. Li, M. Gershow, D. Stein, E. Brandin and J. A. Golovchenko, *Nat. Mater.*, 2003, **2**, 611–615.
4 P. Chen, E. Brandin, Y. R. Kim, Q. Wang and D. Branton, *Nano Lett.*, 2004, **4**, 2293–2298.
5 R. M. M. Smeets, U. F. Keyser, D. Krapf, M. Y. Wu, N. H. Dekker and C. Dekker, *Nano Lett.*, 2006, **6**, 89–95.
6 A. J. Storm, J. H. Chen, H. W. Zandbergen and C. Dekker, *Phys. Rev. E: Stat., Nonlinear, Soft Matter Phys.*, 2005, **71**, 051903.
7 S. Howorka and Z. Siwy, *Chem. Soc. Rev.*, 2009, **38**, 2360–2384.
8 C. Dekker, *Nat. Nanotechnol.*, 2007, **2**, 209–215.
9 A. J. Haes, S. Zou, G. C. Schatz and R. P. Van Duyne, *J. Phys. Chem. B*, 2004, **108**, 109–116.
10 J. D. Uram, K. Ke, A. J. Hunt and M. Mayer, *Small*, 2006, **2**, 967–972.
11 W. Guo, Y. Tian and L. Jiang, *Acc. Chem. Res.*, 2013, **46**, 2834–2846.
12 W. Guo, L. Cao, J. Xia, F.-Q. Nie, W. Ma, J. Xue, Y. Song, D. Zhu, Y. Wang and L. Jiang, *Adv. Funct. Mater.*, 2010, **20**, 1339.
13 J. Gao, W. Guo, D. Feng, H. Wang, D. Zhao and L. Jiang, *J. Am. Chem. Soc.*, 2014, **136**, 12265–12272.
14 L. Cao, W. Guo, Y. Wang and L. Jiang, *Langmuir*, 2012, **28**, 2194–2199.
15 L. Cao, W. Guo, W. Ma, L. Wang, F. Xia, S. Wang, Y. Wang, L. Jiang and D. Zhu, *Energy Environ. Sci.*, 2011, **4**, 2259–2266.
16 D. Fologea, M. Gershow, B. Ledden, D. S. McNabb, J. A. Golovchenko and J. Li, *Nano Lett.*, 2005, **5**, 1905–1909.
17 B. N. Anderson, M. Muthukumar and A. Meller, *ACS Nano*, 2013, **7**, 1408–1414.
18 D. Fologea, J. Uplinger, B. Thomas, D. S. McNabb and J. Li, *Nano Lett.*, 2005, **5**, 1734–1737.
19 N. Hu, Y. Ai and S. Qian, *Sens. Actuators, B*, 2012, **161**, 1150–1167.
20 R. Karnik, R. Fan, M. Yue, D. Y. Li, P. D. Yang and A. Majumdar, *Nano Lett.*, 2005, **5**, 943–948.
21 S. Mafe, J. A. Manzanares and P. Ramirez, *J. Phys. Chem. C*, 2010, **114**, 21287–21290.
22 S.-W. Nam, M. J. Rooks, K.-B. Kim and S. M. Rossnage, *Nano Lett.*, 2009, **9**, 2044–2048.
23 Y. He, M. Tsutsui, C. Fan, M. Taniguchi and T. Kawai, *ACS Nano*, 2011, **5**, 5509–5518.
24 E. B. Kalman, O. Sudre, I. Vlassiouk and Z. S. Siwy, *Anal. Bioanal. Chem.*, 2009, **394**, 413–419.
25 P.-c. Yen, C.-h. Wang, G.-J. Hwang and Y. C. Chou, *Rev. Sci. Instrum.*, 2012, **83**, 034301.
26 K.-H. Paik, Y. Liu, V. Tabard-Cossa, M. J. Waugh, D. E. Huber, J. Provine, R. T. Howe, R. W. Dutton and R. W. Davis, *ACS Nano*, 2012, **6**, 6767–6775.
27 S. Wu, F. Wildhaber, A. Bertsch, J. Brugger and P. Renaud, *Appl. Phys. Lett.*, 2013, **102**, 213108.
28 L.-J. Cheng and L. J. Guo, *Chem. Soc. Rev.*, 2010, **39**, 923–938.
29 I. Vlassiouk and Z. S. Siwy, *Nano Lett.*, 2007, **7**, 552–556.
30 R. Yan, W. Liang, R. Fan and P. Yang, *Nano Lett.*, 2009, **9**, 3820–3825.
31 K. P. Singh and M. Kumar, *Lab Chip*, 2012, **12**, 1332–1339.
32 Y. Ai, J. Liu, B. Zhang and S. Qian, *Sens. Actuators, B*, 2011, **157**, 742–751.
33 A. Nikolaev and M. E. Gracheva, *J. Comput. Electron.*, 2014, **13**, 818–825.
34 S.-H. Lee, H. Lee, T. Jin, S. Park, B. J. Yoon, G. Y. Sung, K.-B. Kim and S. J. Kim, *Nanoscale*, 2015, **7**, 936–946.
35 Z. Jiang and D. Stein, *Langmuir*, 2010, **26**, 8161–8173.
36 Z. Jiang and D. Stein, *Phys. Rev. E: Stat., Nonlinear, Soft Matter Phys.*, 2011, **83**, 031203.
37 S. Xue, L.-H. Yeh, Y. Ma and S. Qian, *J. Phys. Chem. C*, 2014, **118**, 6090–6099.
38 J. Cervera, B. Schiedt, R. Neumann, S. Mafe(é) and P. Ramirez, *J. Chem. Phys.*, 2006, **124**, 104706.
39 R. B. Schoch, J. Han and P. Renaud, *Rev. Mod. Phys.*, 2008, **80**, 839–883.
40 D. Constantin and Z. S. Siwy, *Phys. Rev. E: Stat., Nonlinear, Soft Matter Phys.*, 2007, **76**, 041202.
41 Z. Todorovic and S. K. Milojic, *J. Serb. Chem. Soc.*, 2004, **69**, 1063–1072.
42 N. Sahai and D. A. Sverjensky, *Geochim. Cosmochim. Acta*, 1997, **61**, 2801–2826.
43 S. H. Behrens and D. G. Grier, *J. Chem. Phys.*, 2001, **115**, 6716–6721.
44 X. Liu, J. Cheng, X. Lu and R. Wang, *Phys. Chem. Chem. Phys.*, 2014, **16**, 26909–26916.
45 J. Bai, D. Wang, S.-w. Nam, H. Peng, R. Bruce, L. Gignac, M. Brink, E. Kratschmer, S. Rossnagel, P. Waggoner, K. Reuter, C. Wang, Y. Astier, V. Balagurusamy, B. Luan, Y. Kwark, E. Joseph, M. Guillorn, S. Polonsky, A. Royyuru, S. P. Rao and G. Stolovitzky, *Nanoscale*, 2014, **6**, 8900–8906.
46 S.-W. Nam, M.-H. Lee, S.-H. Lee, D.-J. Lee, S. M. Rossnagel and K.-B. Kim, *Nano Lett.*, 2010, **10**, 3324–3329.
47 A. Uddin, S. Yemenicioglu, C.-H. Chen, E. Corigliano, K. Milaninia and L. Theogarajan, *Nanotechnology*, 2013, **24**, 155501.